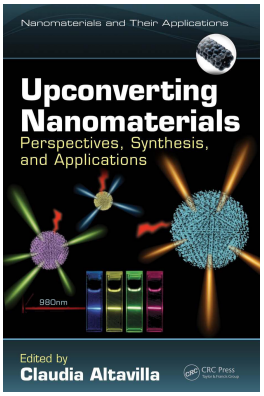

Upconverting Nanomaterials
Perspectives, Synthesis, and Applications

Claudia Altavilla

Synthesis of Upconverting Nanomaterials: Designing the Composition and Nanostructure

Publication details
https://test.routledgehandbooks.com/doi/10.1201/9781315371535-5
Adolfo Speghini, Marco Pedroni, Nelsi Zaccheroni, Enrico Rampazzo
Published online on: 10 Oct 2016

3

Synthesis of Upconverting Nanomaterials: Designing the Composition and Nanostructure

Adolfo Speghini, Marco Pedroni, Nelsi Zaccheroni, and Enrico Rampazzo

CONTENTS

3.1 Introduction

Lanthanide-doped upconverting nanostructures are promising materials in the generation of imaging agents for modern biomedical applications, in particular in optical diagnostics (Prodi et al. 2015). Upconversion (UC) is a

phenomenon involving optical emission at higher energies than that of the exciting radiation, through sequential absorptions of photons. Lanthanide ions are particularly useful for this process, due to a peculiar energy levels scheme and relatively long-excited states lifetimes (Auzel 2004). In the past decades, many hosts and types of lanthanide ions have been chosen to customize the luminescence properties of the nanosystems, tailoring also their structure to fit efficiently the final application. In this context, some reviews have appeared in the literature describing preparation of lanthanide-doped nanocrystals (DaCosta et al. 2014; Gainer and Romanowski 2014; Hemmer et al. 2013; Y. Liu et al. 2013; Wang and Liu 2009; Yang et al. 2014; Zhou et al. 2012) evidencing the high interest and activity of the field. In these reviews, several factors such as morphology, crystalline phase, size, and components of these nanomaterials have been demonstrated to be crucial parameters acting on their electrical, photophysical, magnetic, and colloidal stability properties (Sun et al. 2014; van Veggel et al. 2012), see Figure 3.1.

The target of this chapter is to briefly illustrate the diverse synthesis of UC nanomaterials, with particular attention to the composition of the host and to the architecture of the nanostructures, tailored to produce efficient luminescent nanomaterials.

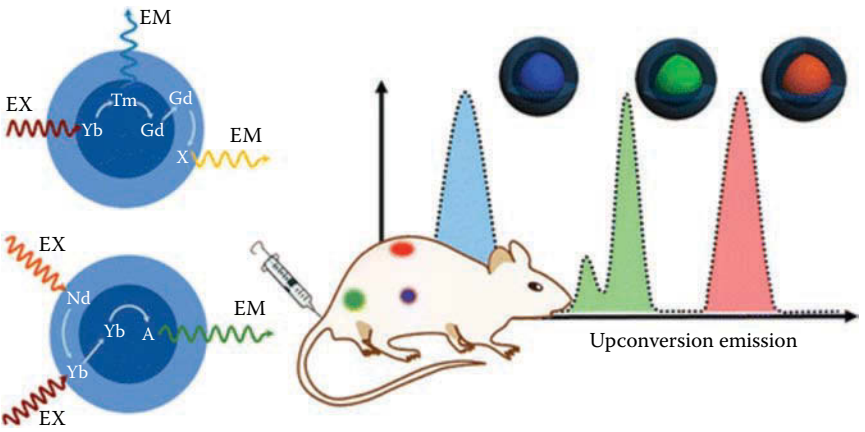

FIGURE 3.1
UC emission obtained from RE nanoparticles with controlled size and structure can be used for many biological applications, thanks to multicolor and tunable emissions. These rationally designed nanostructures and nanocomposites can be engineered to meet various applications, such as imaging, detection, and sensing. (Reprinted with permission from Sun, L. D., Y. F. Wang, and C. H. Yan. 2014. Paradigms and challenges for bioapplication of rare earth upconversion luminescent nanoparticles: Small size and tunable emission/excitation spectra. *Acc. Chem. Res.* 47:1001–1009. Copyright 2014 American Chemical Society.)

3.2 Upconverting Nanomaterials: Importance of the Composition

Among the factors affecting the UC properties of nanomaterials, the choice of the species that absorb (sensitizers) and emit (activators) the radiation is of paramount importance. The mainly exploited sensitizer is Yb^{3+}, characterized by a single transition in the near-infrared (NIR) range, around 980 nm, ($^2F_{7/2} \rightarrow {}^2F_{5/2}$ transition) closely matching the energies of the excited states of several activator ions such as Er^{3+}, Tm^{3+}, and Ho^{3+}. The doping amounts of both sensitizer and activator ions define the luminescence features of the nanomaterials, since they have to be optimized taking into account the delicate balance between the quite high amount required to favor energy transfer toward the activator, and the prevention of detrimental cross-relaxation processes (Mita et al. 1995).

Appropriate selection of suitable host materials for efficient UC emission is also of paramount importance. Important properties of these hosts are

- High chemical stability
- High transparency in the optical range of interest (in ultraviolet (UV), visible, and NIR ranges)
- High optical damage threshold

Moreover, the UC emission efficiency strongly depends on the vibrational properties of the host, influencing nonradiative relaxations for the excited states of the emitting lanthanide ions. The latter processes involve multiphonon assisted deactivation processes, in which the phonons are bridging the energy gap between the emitting level and the next lower lying energy level of the lanthanide ion. As a general rule, the larger is the number of phonons needed to bridge this energy gap and the higher is the efficiency of the radiative emission (Chen et al. 2013). Therefore, to increase the UC emission efficiency, it is desirable to have lanthanide ions embedded in a host for which the phonon energies are as low as possible. The cutoff phonon energy depends on the type of host, and in general, fluoride-based materials have lower phonon energies than oxide compounds (Chen et al. 2014). For instance, cutoff phonon energies for Y_2O_3 (Vetrone et al. 2004) (around 500 cm^{-1}) and ZrO_2 (Patra et al. 2003a) (around 550 cm^{-1}) are much higher than for $NaYF_4$ (Ivaturi et al. 2013) (around 350 cm^{-1}). The efficiency of a UC emission is also strongly dependent on the local symmetry of the site in which the lanthanide ion is accommodated (Peacock 1975). Due to the peculiar character of lanthanide 4f–4f transitions, a lower local symmetry is favorable for increasing the emission efficiency (Krämer et al. 2004; Lin et al. 2014; Schafer et al. 2009).

3.3 Synthetic Strategies

The development of synthetic strategies for efficient luminescent nanomaterials with defined size, shape, composition, and phase is of paramount importance. This section is devoted to the description of the most popular synthetic methods approaches to obtain tailored nanomaterials in a facile and controlled way. We will mainly focus on the advantages (pros) and disadvantages (cons) for each approach and in order to help the reader in the comparison, we have summarized the main features in Table 3.1.

3.3.1 Coprecipitation

The coprecipitation method is characterized by simple protocols, quite short reaction times, simple reaction conditions, and cheap experimental setups.

TABLE 3.1

Overview of the Synthetic Methods Used for the Preparation of Different Hosts with Advantages (Pros) and Disadvantages (Cons)

Synthetic Methods	Hosts (Examples)	Pros	Cons
Coprecipitation	LaF_3, $NaYF_4$, GdF_3 Y_2O_3, Lu_2O_3, $Gd_3Ga_5O_{12}$ $LuPO_4$ $YbPO_4$ GdOF, $Gd_4O_3F_6$ $Lu_6O_5F_8$	• Short preparation time • Relatively cheap and facile procedure	• High T treatment • Poor size control • Aggregation
Thermolysis	LaF_3, $NaYF_4$, $NaGdF_4$ Y_2O_3, Gd_2O_3 LaOF, GdOF	• High quality • Good size and crystallinity control • Low aggregation	• Costly and demanding procedures • High T treatment • Toxic by-products
Solvo(hydro) thermal	$NaYF_4$, $NaLuF_4$ YbF_3, YF_3, GdF_3 CaF_2, SrF_2, $CaGd_3F_{11}$ Gd_2O_3, Er_2O_3	• Relatively mild T • High quality • Good size control • Good dopant control • Low amount of toxic by-products	• Relatively long preparation time
Sol–gel	ZrO_2, $BaTiO_3$, TiO_2 Titanates (nanotubes) Y_2O_3, Gd_2O_3, $Lu_3Ga_5O_{12}$ YVO_4	• Low amount of toxic by-products • Relatively facile procedures	• Final calcination • Aggregation • Relatively long preparation time
Combustion	Y_2O_3, Lu_2O_3, Gd_2O_3 $Gd_3Ga_5O_{12}$	• Short reaction times	• Very high T
ILs	YF_3, GdF_3, EuF_3 $NaYF_4$, $NaGdF_4$	• A "green" approach	• Aggregation

In this procedure, the nucleation of the nanocrystals can be promoted using capping agents (such as polyvinylpyrrolidone (PVP) or polyethyleneimine (PEI)). In some cases, the nanoparticles (NPs) are directly generated without the need of postformation heat treatments, in others cases, annealing is necessary to obtain the desired phase.

3.3.1.1 Fluorides

First examples were published by Van Veggel and coworkers, that synthesized LaF_3 nanoparticles, containing emitters such as Eu, Er, Nd, and Ho, using di-n-octadecyldithiophosphate as a surfactant (Stouwdam and van Veggel 2002) and by Cho et al. (Yi and Chow 2005), who obtained a very small particle size (around 5 nm), with NPs easily dispersible in water.

To prepare the most famous UC phosphor $NaYF_4$, other authors used relatively low reaction temperatures using amines as solvents (Heer et al. 2004). Yi et al. (2004) used and lanthanide–ethylenediaminetetraacetic acid (EDTA) complexes as starting material. The tuning of the molar ratio of EDTA to total lanthanides allowed the control of nanoparticle size from 40 to 170 nm, but samples were affected by low luminescence emission efficiency and rather poor monodispersion. Other approaches succeeded in developing hexagonal-phase $NaYF_4$:Yb,Er/Tm nanocrystals with tunable sizes: these systems were formed starting from small amorphous $NaYF_4$ nanoparticles obtained by precipitation, and by a subsequent treatment at higher temperature (300°C), and showed higher up-conversion emission efficiency (Li and Zhang 2008; Li et al. 2008).

Hollow mesoporous GdF_3 nanoparticles were prepared also by coprecipitation method by Lv et al. (2013) using pH controlled solutions.

3.3.1.2 Oxides

Sesquioxides have been prepared by this method. For instance, Er^{3+}, Yb^{3+} codoped Y_2O_3 upconverting nanoparticles (UCNPs) have been prepared by using a coprecipitation method followed by a postthermal treatment, using a surfactant (cetyltrimethylammonium bromide, CTAB) that had an important role in controlling the size (Lu et al. 2014). Moreover, Er^{3+}, Yb^{3+} codoped Lu_2O_3 nanoparticles with several sizes and shapes (nano-aggregates, submicrometer wires, and nanospheres) were prepared by the coprecipitation technique. It was found that different reactant ratios of lanthanide to urea precipitant produced uniform spherical nanoparticles with sizes of 45, 100, 165, 200, and 250 nm (Zheng et al. 2014).

Er^{3+}-doped Garnet ($Gd_3Ga_5O_{12}$) nanoparticles were also prepared by Daldosso et al. (2008) by coprecipitation, showing quite good UC emission.

Phosphate nanoparticles were also prepared using the coprecipitation technique by Heer et al. (2003), who published a pioneering paper in 2003 about the synthesis of Tm^{3+}, Yb^{3+}-doped $LuPO_4$, and Er^{3+}-doped $YbPO_4$

nanocrystals in the form of transparent colloidal solutions, demonstrating the possibility of obtaining UC blue, green, and red light emission in transparent colloidal solutions by laser excitation in the near-IR region around 980 nm.

3.3.1.3 Oxyfluorides

Few examples of oxyfluoride UC samples prepared by coprecipitation techniques are reported in the literature. Codoped Er^{3+}, Yb^{3+}, Tm^{3+}/Yb^{3+}, Ho^{3+}/Yb^{3+}, and triply doped $Er^{3+}/Tm^{3+}/Yb^{3+}$ single phase GdOF and $Gd_4O_3F_6$ nanoparticles with average particle sizes around 25 and 50 nm, respectively, were prepared in aqueous solution under alkaline conditions by a simple coprecipitation method and a heat treatment at 500°C (Passuello et al. 2011a, b). Due to the heat treatment, a certain degree of agglomeration was observed. In the case of triply doped samples, the nanoparticles show bright white light UC emission upon excitation at 980 nm using a diode laser as the excitation source.

A series of $Er^{3+}/Tm^{3+}/Yb^{3+}$-doped $Lu_6O_5F_8$ nanoparticles have been prepared by a coprecipitation method (Guo et al. 2013). The average size has been tuned from 20 to 320 nm upon increasing Li^+ ion concentration in the host. The detailed crystal structure of $Lu_6O_5F_8$ was analyzed via Rietveld refinement of the powder x-ray diffraction patterns. It is worth mentioning that Li^+ concentration influences the white UC emission. In this case, Li^+ ion behaves as a luminescence intensifier.

3.3.2 Thermolysis

This synthetic approach is often used to form lanthanide-doped nanoparticles, since it provides high quality nanocrystals, with high control over dimension, monodispersity, and photoluminescence (PL) properties. It involves a heat treatment (~300°C) of lanthanide precursors, usually organometallic compounds (e.g., acetate or trifluoroacetate salts) that decompose in nonpolar high boiling organic solvents, such as oleylamine (OM), trioctylphosphine oxide (TOPO), or 1-octadecene (ODE). Surfactants with capping groups, for instance, oleic acid (OA), are in charge to control the nanoparticle size and to prevent their aggregation, due to long hydrocarbon chains. The main parameters affecting this synthetic approach are reaction temperature, metal precursors and their concentration, nature of the solvent, capping agent(s), and reaction time. By careful tuning of these experimental parameters, highly monodispersed nanoparticles with very good crystallinity have been produced using the thermolysis method. Besides these positive features, the thermolysis method presents some serious drawbacks. In particular, quite expensive procedures with demanding aspects such as high temperatures and air sensitive starting materials handling are involved. Moreover, the formation of highly toxic fluorinated by-products

could limit the large-scale application of this synthetic approach in bio-related applications.

3.3.2.1 Fluorides

A substantial amount of literature has been published in the last 10 years reporting preparation of fluorides with the thermolysis method. One of the first reports was published by Yan et al. (Zhang et al. 2005), who synthesized LaF3 nanocrystals starting from $La(CF_3COO)_3$ salt, using OA as the capping agent and ODE as the high boiling noncoordinating solvent. This method was extended to other lanthanide-doped nanoparticles, for instance, for the preparation of the famous upconverter material, $NaYF_4$, by several groups (Abel et al. 2009; Boyer et al. 2006; G. Chen et al. 2010; Cuccia and Capobianco 2007; Yi and Chow 2006). Also, the group of Murray and co-workers (Ye et al. 2010), succeeded in the synthesis of $NaYF_4$:Yb, Er nanocrystals with a controlled size and morphology (spherical/nanorod): this approach definitely provided a way to high quality and monodipersed colloids. Also Yin et al. (Yu et al. 2010), synthesized monodisperse β-$NaYF_4$:Yb, Tm nanocrystals with controlled size (25–150 nm), composition, and shape (sphere, hexagonal prism, and hexagonal plate) by thermolysis of metal trifluoroacetates in hot solutions (300–330°C) containing OA, OM, and ODE.

Another interesting host for UC emission, $NaGdF_4$, was also prepared in nanocrystalline form using the thermolysis method (see Figure 3.2), by the group of Capobianco et al. (Boyer et al. 2007; Naccache et al. 2009). Other groups (Cichos et al. 2014; Johnson et al. 2011; Liu et al. 2010; Z.-L. Wang et al. 2010; Zhou et al. 2010) have investigated this host, also for its interesting magnetic resonance imaging (MRI) properties.

A general synthesis of high quality cubic and hexagonal $NaREF_4$(RE: Pr to Lu, Y) nanocrystals (nanopolyhedra, nanorods, nanoplates, and nanospheres) and $NaYF_4$:Yb, Er/Tm nanocrystals (nanopolyhedra and nanoplates) via the co-thermolysis of $Na(CF_3COO)$ and $RE(CF_3COO)_3$ in OA/OM/1-ODE was reported (Mai et al. 2006). By tuning the ratio of Na/RE, solvent composition, reaction temperature and time, control of the phase, shape, and size of the nanocrystals has been achieved. Interesting hosts for UC nanomaterials have demonstrated to be the alkaline earth fluorides (D. Chen et al. 2010; Quan et al. 2008). Uniform alkaline earth metal fluoride MF_2(M = Mg, Ca, and Sr) nanomaterials with various shapes (tetragonal MgF_2 nanoneedles; cubic CaF_2 nanoplates and nanopolyhedra; cubic SrF_2 nanoplates and nanowires) have been synthesized from the thermolysis of alkaline earth metal trifluoroacetate in hot surfactant solutions, with OA, OM, and ODE (Du et al. 2009). The MF_2 nanocrystals were formed by the controlled fluorination of the M–O bond into the M–F bond at the nucleation stage and subsequent growth process. In these cases, the growth of shape-selective MF_2 nanocrystals was likely due to the template direction of micellar structures formed by self-assembly of capping ligands and the so-called "Ostwald ripening" process.

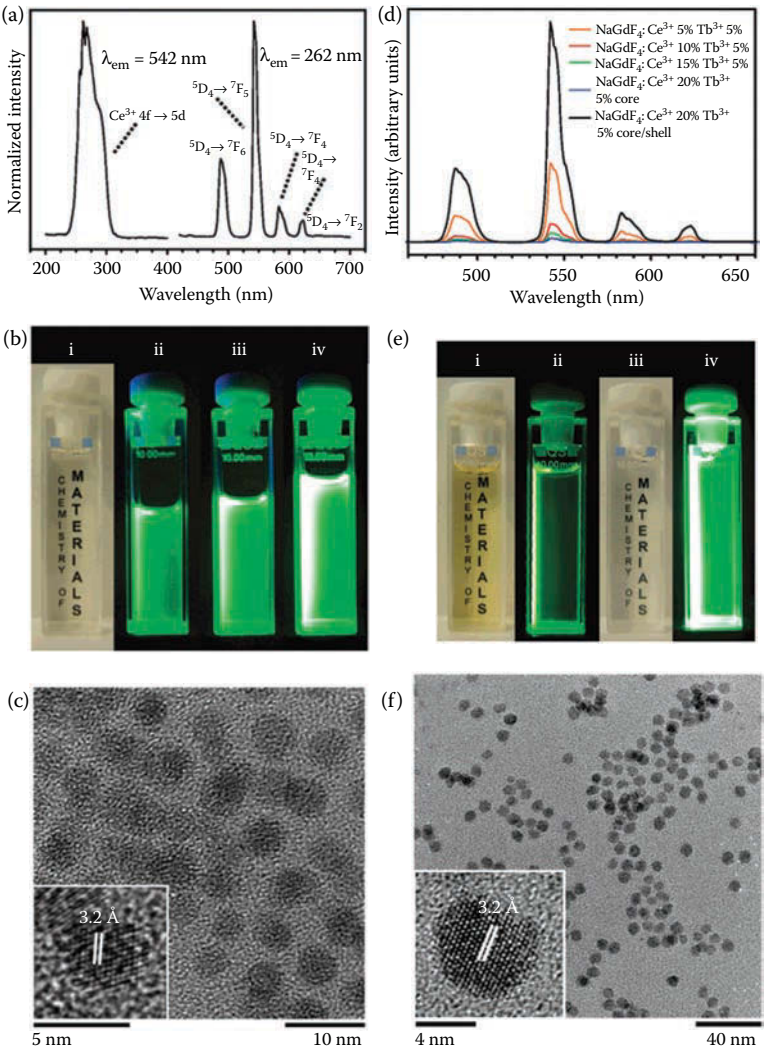

FIGURE 3.2

(a) Excitation and emission spectra of $NaGdF_4$: 15% Ce^{3+}, 5% Tb^{3+} nanoparticles (1 wt% solution in hexane). (b) 1 wt% solution (hexane) of $NaGdF_4$: 10% Ce^{3+}, 5% Tb^{3+} nanoparticles under (i) ambient and (ii) 254 nm UV light. 1 wt% solutions of (iii) $NaGdF_4$: 15% Ce^{3+}, 5% Tb^{3+} and (iv) $NaGdF_4$: 20% Ce^{3+}, 5% Tb^{3+} nanoparticles (hexane) under 254 nm UV light. (c) TEM image of $NaGdF_4$: 20% Ce^{3+}, 5% Tb^{3+}. (d) Emission spectra of 1 wt% solutions (hexane) of $NaGdF_4$:Ce^{3+}, Tb^{3+} core and $NaGdF_4$:Ce^{3+} 20%, Tb^{3+} 5%/$NaYF_4$ core/shell NPs. (e) 1 wt% solution (hexane) of aged $NaGdF_4$: 20% Ce^{3+}, 5%Tb^{3+} nanoparticles under (i) ambient and (ii) 254 nm UV light and $NaGdF_4$: 20% Ce^{3+}, 5% Tb^{3+}/$NaYF_4$ nanoparticles under (iii) ambient and (iv) 254 nm UV light. (f) TEM image of $NaGdF_4$: 20% Ce^{3+}, 5% Tb^{3+}/$NaYF_4$ sample. (Reprinted with permission from Boyer, J. C., J. Gagnon, L. A. Cuccia, and J. A. Capobianco. 2007. Synthesis, characterization, and spectroscopy of $NaGdF_4$: Ce^{3+}, Tb^{3+}/$NaYF_4$ core/shell nanoparticles. *Chem. Mater.* 19 (14):3358–3360. Copyright 2007 American Chemical Society.)

3.3.2.2 Oxides

Some examples are reported in the literature describing the preparation of sesquioxides using a thermolysis method. Well-dispersed Y_2O_3 nanocrystals, with a size less than 10 nm, and self-assembled nanodisks have been synthesized by a simple organometallic route using OM (H. Wang et al. 2005), in which TOPO was added to improve the crystallinity.

Furthermore, monodisperse cubic sesquioxides (from La to Lu and Y) nanomaterials (in the form of ultrathin nanoplates and nanodisks) have been synthesized via a nonhydrolytic approach in OA/OM/ODE (Si et al. 2007). Several lanthanide complexes, such as acetylacetonate, benzoylacetonate, and acetate, have been considered as precursors. The transformation from the complex precursors to the sesquioxides was proposed to occur in two stages: first, the formation of rare earth (RE) oleates by ligand exchange in solution and second, the subsequent decomposition of the oleates into sesquioxides catalyzed by OM.

Gd_2O_3 nanoplates were synthesized by solution-phase decomposition of gadolinium-acetate precursors in the presence of both coordinating and noncoordinating solvents, such as OM, OA, and ODE (Cao 2004).

3.3.2.3 Oxyfluorides

Monodispersed RE oxyfluoride nanocrystals with diverse shapes (cubic RE oxyfluoride nanopolyhedra and nanorods) have been prepared from single-source precursors of metal acetates through controlled fluorination in OA/OM/ODE (Sun et al. 2007). To selectively obtain RE oxyfluoride nanocrystals, the fluorination of the RE–O bond to the RE–F bond at the nucleation stage was controlled by finely tuning the ratio of OA/ODE or OA/OM, and the reaction temperature. Tuning of their shape has been realized by further modifying the reaction conditions. Monodispersed cubic phase LaOF and GdOF nanostructures were prepared by decomposing the lanthanide trifluoroacetate precursors in OA and OM (Du et al. 2008). Nanocrystals from 2 to 7 nm size and various shapes (nanopolyhedra and elongated nanocrystals) have been obtained.

3.3.3 Solvo(hydro)thermal

The hydro-solvothermal strategy requires relatively low temperatures (usually <250°C) taking advantage of experimental setups involving an autoclave reactor. Despite the mild conditions, the method allows one to obtain nanoparticles with a good level of crystallinity, with good control over dimension and morphology by fine tuning the experimental temperature and reaction time, the nature of the solvent and the surfactant and their molar ratios. As an important advantage with respect to the thermolysis method, it produces a lower amount of toxic by-product. Organic solvents as alcohols or

amines are used in the presence of surfactant additives such as OA, EDTA, CTAB, or PEI: nonetheless, water is frequently used as well.

3.3.3.1 Fluorides

One of the first examples of production of upconverting $NaYF_4$ nanoparticles by the hydrothermal method is reported by Zeng et al. (2005). The solutions containing the metal precursors were transferred to a Teflon-lined autoclave and heated to 140–200°C for 12–24 h. The author succeeded in controlling the size and morphology of the products by the addition of EDTA and CTAB. $NaYF_4$ nanoparticles were also prepared by this method by several other authors, for instance, by Zhao et al. (2008) who prepared Yb^{3+} and Er^{3+} codoped cubic and hexagonal-phase $NaYF_4$ nanoparticles in different shapes, using a citrate–yttrium-nitrate complex as the precursor and a treatment in autoclave at different temperatures and reaction times. Citric acid was also used as a capping agent by Jiang et al. (2012), that prepared Tm^{3+}, Yb^{3+} codoped α-$NaYF_4$ nanocrystals by a one-step hydrothermal method. The morphology of the nanomaterials maintains a spherical shape when the surfactant amount, hydrothermal time, and hydrothermal temperature were varied. Quite interestingly, under 980 nm excitation, intense UV and blue UC emissions were observed from the α-$NaYF_4$ nanoparticles.

Hao and coworkers synthesized via a hydrothermal method (ethanol–water, OA 170°C, 24 h) fluorescent and magnetic (MRI) $NaLuF_4$:Ln (Ln = Gd^{3+}, Yb^{3+}, Tm^{3+}) nanocrystals with efficient NIR-to-NIR emission, useful for *in vivo* imaging applications. Interestingly, they were able to tune the crystal phase, size, UC properties, and magnetization varying the Gd^{3+} doping degree (Zeng et al. 2012).

One approach proposed as a general strategy to develop nanomaterials, exploits a phase transfer and separation mechanism occurring at the interfaces of the liquid, solid, and solution (LSS) phases present during the synthesis (X. Wang et al. 2005). In the case of lanthanide-doped luminescent nanocrystals with UC emission properties, the reaction between NaF and Ln acetate salts at 180°C was used to obtain approximately round-shaped nanoparticles of $NaYF_4$, YbF_3, LaF_3 (4–12 nm), or oval ones of YF_3 (100 × 500 nm). This strategy was subsequently implemented by Liu and coworkers (F. Wang et al. 2010), that showed how $NaYF_4$ nanocrystals can be rationally tuned in size, phase (cubic/hexagonal), and emission color using trivalent lanthanide dopant ions at controlled concentrations. The reaction time (~2 h) and phase transition occurred at quite moderate reaction temperature (~230°C). The LSS method was also applied to the synthesis of ultra-small (~5 nm) SrF_2 nanocrystals using trivalent lanthanide ions (Ln^{3+}) as doping agents at a concentration up to 40% (mol/mol) (D. Chen et al. 2010). Moreover, with the same wet chemical LSS technique, upconverting monodispersed Yb^{3+}/Er^{3+}-doped CaF_2 nanoparticles have been prepared (G. Wang et al. 2009). The obtained nanomaterials not only can be transparently dispersed in

cyclohexane but also can be converted into water-soluble ones by oxidizing OA ligands with the Lemieux-von Rudloff reagent. Very interestingly, upon 980 nm laser excitation, the colloidal dispersion in cyclohexane and water showed bright green UC luminescence (UCL), even slightly stronger that of Yb^{3+}/Er^{3+}-doped $NaYF_4$ nanocrystals.

A facile method for the synthesis of polyethylene glycol (PEG) capped, water dispersible lanthanide-doped UC GdF_3 NPs using a hydrothermal technique was adopted by Passuello et al. (2012). From the investigation, it was found that the layer of PEG coating of the GdF_3 NPs guaranteed a good dispersion of the nanostructure in water and increased the UC emission by decreasing the multiphonon relaxation of the excited states of the Er^{3+} and Tm^{3+} ions due to water phonons.

Er^{3+}/Yb^{3+}, Ho^{3+}/Yb^{3+}, and Tm^{3+}/Yb^{3+} codoped CaF_2 of cubic shape NPs have been prepared by a one-step hydrothermal technique by Pedroni et al. (2011) in water using sodium oleate as surfactant. The obtained NPs were easily dispersed in organic solvents as well as in oleate aqueous solutions, without the need for any postsynthesis reaction. Notably, the Ho^{3+}/Yb^{3+} and Tm^{3+}/Yb^{3+}-doped samples show strong UC emission in the 750–800 nm region upon 980 diode laser excitation, a useful range for biomedical applications. Using the same hydrothermal technique, Tm^{3+}/Yb^{3+}-doped CaF_2 and SrF_2 were directly obtained using citrate anions as capping agents (Pedroni et al. 2013). Colloidal water dispersions of the doped SrF_2 NPs showed a UC emission at 800 nm (due to Tm^{3+} ions) of about two orders of magnitude higher than similarly doped cubic phase $NaYF_4$ NPs prepared with the same hydrothermal technique. It was found that alkali ions (Na^+ or K^+), present as counter cations of the citrate salts used as precursors, can be incorporated in the fluoride host crystals as charge compensators and they have a strong influence of the spectroscopic properties of the lanthanide ions.

A shape-controlled synthesis of monodispersed Yb^{3+} and Er^{3+}-doped $CaGd_3F_{11}$ nanoparticles using a solvothermal method was recently reported by Tian et al. (2014). The morphology of the nanostructures can be tuned to spherical (<10 nm) and one-dimensional nanorods by varying the amounts of the solvents and capping agent in the starting solution. UC emission was found to depend from the shapes of the obtained $CaGd_3F_{11}$ nanoparticles and nanorods, in particular, the nanorods showed a brighter emission with respect to the nanoparticles.

3.3.3.2 Oxides

Hydrothermal synthesis (water, pH = 13, 24 h at 180°C), followed by calcination (800°C) was also used by Qu and coworkers (Z. Liu et al. 2013) to form sesquioxides nanoparticles. In particular, they reported about the synthesis of multimodal PEGylated Gd_2O_3:Yb^{3+}, Er^{3+} nanorods (PEG-UCNPs) for *in vivo* UCL, T_1-enhanced magnetic resonance, and x-ray computed tomography imaging. PEGylation was introduced using a trialkoxysilane-PEG, conferring

long blood circulation time, stability *in vivo* and noncytotoxic character, as indicated by small-animal experiments. With two different ligands—OA and aminohexanoic acid (AA)—Li and coworkers (Cao et al. 2011) succeeded in the hydrothermal synthesis of high quality water-soluble UC nanocrystals bearing appropriate functional groups using a one-step synthetic strategy. The OA/AA molar ratio allowed to optimize water dispersibility and provided amino groups for conjugation to folic acid (FA) for targeted bioimaging (Figure 3.3).

An interesting approach for the synthesis of cubic Er_2O_3 nanostructures with high yield and controlled size and shape has been developed via a solvothermal reaction of erbium nitrate in water/ethanol/decanoic acid media (Nguyen et al. 2010). The cubic Er_2O_3 phase was obtained at a temperature lower than 200°C and by tuning experimental parameters (such as the reaction temperature, the concentration of decanoic acid, and erbium precursor), different sizes and a variety of sheaves and brooms can be obtained. Furthermore, a change of the solvent (anhydrous ethanol instead of water/ethanol) had a strong influence on the particle size. Interestingly, at high precursor concentrations, nanorods were formed due to anisotropic

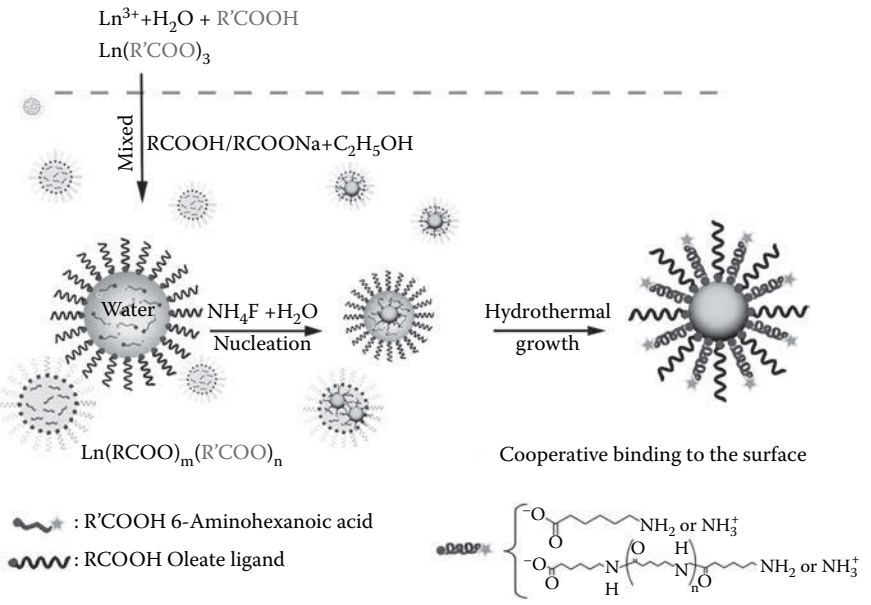

FIGURE 3.3
Scheme of hydrothermal reaction for preparing amino-functionalized UCNPs assisted with binary cooperative ligands: hydrophilic 6-AA and hydrophobic oleate. (Reprinted from *Biomaterials*, 32 (11), Cao, T. Y., Y. Yang, Y. A. Gao, J. Zhou, Z. Q. Li, and F. Y. Li, High-quality water-soluble and surface-functionalized upconversion nanocrystals as luminescent probes for bioimaging, 2959–2968, Copyright 2011, with permission from Elsevier.)

growth. It was found that the UCL properties depend on the particle size of the products.

3.3.4 Sol–Gel

The sol–gel technique has been considered by some groups in the past years to prepare oxide-based UC nanomaterials and it is characterized by hydrolysis and polycondensation of metal alkoxide (or halide)-based precursors. On the other hand, in order to improve the crystallinity of the nanosized materials, a further heat treatment at relatively high temperatures is often carried out. Due to this treatment, the obtained nanoparticles present considerable aggregation, and well-dispersed water solutions are therefore hard to prepare, making their application in the biomedical field difficult. Nonetheless, these NPs can be considered for other applications not requiring very homogeneous dispersions.

An interesting upconverting material is lanthanide-doped ZrO_2. De la Rosa et al. prepared Er^{3+}-doped zirconium oxide using the sol–gel process (De la Rosa-Cruz et al. 2003), followed by an annealing treatment at 1000°C for 10 h. It was found that the crystallite sizes presented dependence from the Er^{3+} concentration in the host, ranging from 28 to 46 nm. UC in the green and red regions were observed with NIR excitation and the intensity of the UC emission bands varied with the Er^{3+}concentration in the host. Moreover, Prasad et al. investigated an interesting modification of the sol–gel technique to generate Er^{3+}-doped ZrO_2 nanoparticles, considering a sol–emulsion–gel technique that used reverse micelles formed in emulsions as reactors for the growth of the nanocrystals (Patra et al. 2002). The authors also studied the effects of the Er^{3+} concentration and different codopants (e.g., Yb^{3+} and Y^{3+}) in the ZrO_2 host on the UC emission. Green and red UC emission at 550 and 670 nm were observed from these oxide nanocrystals upon excitation at 980 nm, the total UC in the green and red regions decreases with increasing concentration of Er^{3+} ions in the host, while it increased with the presence of Y^{3+} and Yb^{3+} ions.

Other binary oxides as TiO_2 have revealed to be interesting as hosts for UC emission. Luo et al. (2011) prepared Er^{3+}-doped anatase TiO_2 nanoparticles via a sol–gel solvothermal method. From emission and excitation spectra as a function on the temperature in the 10–300 K range, a crystal-field (CF) analysis for the Er^{3+} ions assuming a C_{2v} site symmetry revealed a relatively large CF strength (549 cm^{-1}). The UC intensity in Yb^{3+}, Er^{3+} codoped nanoparticles was about five times higher than for Er^{3+} singly doped counterparts, due to efficient Yb^{3+} sensitization and energy transfer UC (ETU).

Patra et al. (2003b) investigated the effects of the Er^{3+} concentration, crystal size and phase, and different processing temperatures on the UC emission for Er^{3+}-doped $BaTiO_3$ and TiO_2 nanocrystals, using a sol–emulsion–gel technique. Using the same experimental setup conditions, and the same Er^{3+} concentration, the observed UC intensity was higher for $BaTiO_3$ than for the TiO_2 host. For the TiO_2 host, the highest UC intensity was observed for samples

heat treated at 800°C, where both the anatase and rutile phases were present. From an analysis of UC spectra and power studies, it was confirmed that UC emission was produced by excited-state absorption (ESA) processes.

The preparation of Ho^{3+}, Yb^{3+}-doped titanate nanotubes was carried out by Pedroni et al. (2012) via a two-step procedure: a first sol–gel process to produce the lanthanide-doped titania and a second hydrothermal treatment in alkaline conditions on the obtained doped titania powders to form the titanate nanotubes. A treatment at various temperatures was carried out with the aim of determining the different structural and optical properties of the nanotubes. It was found that on increasing the heat treatment the nanotube UC was stronger, due to reduction of hydroxyl groups and water on the surface of the nanotubes, resulting in changes in the interlayer distances.

Er^{3+} and Yb^{3+}, Er^{3+}-doped Y_2O_3 core–shell particles were synthesized by Dorman et al. (2012) with a two-step process, where the cores were prepared by a molten salt technique and the shell was deposited with a sol–gel process. The authors succeeded inpreparing cores with sizes of 100–150 nm, and shell layers up to 12 nm thick, tunable by controlling the mass ratio between the lanthanide chlorides used as precursors and the core (Er^{3+}-doped Y_2O_3) nanoparticles. A Y_2O_3 shell layer with optimal thickness of 8 nm induced a 53% increase in luminescence lifetimes and visible separation in Stark splitting. Optically active-shell layers, as Yb_2O_3 and Yb^{3+}-doped yttria, also facilitated energy transfer between the lanthanide ions, and it was found that Yb_2O_3 is an interesting host for the shell and it produce an increased lifetime and low pump power needed for UC. Lu et al. (2008) investigated Tm^{3+}, Yb^{3+}-doped Y_2O_3 NPs synthesized with the Pechini sol–gel technique, and coated with SiO_2 or TiO_2 shells using the Stober method. Larger NPs have stronger UC emission than smaller NPs and the core–shell structures are useful to enhance the UCL.

Guo et al. (2004) have investigated the UC properties of other sesquioxides, such as Tm^{3+}, Er^{3+}, and Yb^{3+}-doped cubic phase Gd_2O_3 nanoparticles, prepared by the sol–gel technique. UC emission upon 980 nm laser excitation has been observed in the blue, green, and red regions with a relevant increase of the red emission with respect to the green one.

Nanocrystalline lanthanide-doped $Lu_3Ga_5O_{12}$ garnets have been prepared using a sol–gel technique and subsequent heat treatment at 900°C for 16 h in air, by Venkatramu et al. (2010). The aggregated nanomaterials showed an average particle size of 40 nm. These materials show higher luminescence intensities compared to that found for similarly doped sesquioxides (e.g., Y_2O_3) but also for other nanocrystalline garnets, as $Gd_3Ga_5O_{12}$ and $Y_3Al_5O_{12}$.

An interesting investigation on films composed by nanocrystalline lanthanide-doped YVO_4 nanoparticles was carried out by Yu et al. The films were prepared with a combined use of a Pechini sol–gel process and soft lithography (Yu et al. 2002). From x-ray diffraction analysis, it was found that the films began to crystallize at 400°C and the crystallinity was found to increase on increasing of the annealing temperatures. Starting from nonpatterned

phosphor films, mainly consisting of grains with an average size of 90 nm, crystalline films of different thicknesses were obtained. Quite interestingly, the Sm^{3+}-doped YVO_4 films also showed UCL upon laser excitation at 940 nm. In particular, anti-Stokes emissions from the $^4G_{5/2}$ excited state to the lower lying $^6H_{5/2}$, $^6H_{7/2}$, and $^6H_{9/2}$ states have been observed. As the $^6F_{11/2}$ level of Sm^{3+} has a very short lifetime, ESA transitions starting from the $^6F_{11/2}$ energy level have a low probability and the authors proposed that the most probable UC mechanisms could be an energy transfer between Sm^{3+} ions.

3.3.5 Combustion

Combustion synthesis includes controlled explosion reactions and one important advantage of this technique is that the reaction products can be generated in few minutes. Usually, these reactions involve highly exothermic processes that are started by a heat source, to reach temperatures up to 3000°C in the form of a self-sustained combustion propagating through the materials. This technique is most usually considered to synthesize oxide-based upconverting nanoparticles.

Upconverting lanthanide-doped sesquioxides (e.g., Y_2O_3, Lu_2O_3, and Gd_2O_3) prepared by the combustion (or propellant) technique have been investigated by Capobianco et al. in several papers published in the last decade. The first paper on upconverting Er^{3+}-doped nanocrystalline Y_2O_3 appeared in the literature in the year 2000, describing the UC emission of the Er^{3+} ions under laser excitation at 815 nm (Capobianco et al. 2000). The sample was prepared by combustion synthesis, using glycine as a fuel. A further heat treatment at 500°C was needed to decompose the residual nitrate ions. The decay times for the Er^{3+} excited levels obtained for the nanocrystalline sample were found to be in general significantly longer than those observed for the bulk counterpart, due to increased multiphonon relaxation caused by CO_2 and water absorbed onto the surface of the nanosized sample. The same preparation technique was also used to prepare Ho^{3+}-doped Y_2O_3 nanopowders, in order to compare the UC properties with those of the bulk counterpart.

An interesting analysis about the morphological structure of lanthanide-doped Lu_2O_3 powders obtained by propellant synthesis has been carried out by Polizzi et al. (2004). The samples showed a very porous, open morphology with fractal scaling properties. The building blocks of the fractal aggregates are lanthanide-doped cubic Lu_2O_3 crystalline particles with 60–90 nm of average size, which exhibit changes in the lattice parameter proportional to the lanthanide ionic radius. A similar morphological structure was also found for nanocrystalline Y_2O_3 prepared with the same combustion method (Polizzi et al. 2001).

The spectroscopic properties of Er^{3+}, Yb^{3+}-doped Gd_2O_3 nanoparticles prepared by combustion synthesis have been investigated by Singh et al. (2008, 2009), the samples were prepared using urea as the fuel. The solution

containing the precursors was heated at 60°C to evaporate water, becoming a gel and this gel was transferred to a furnace and maintained at 500°C until the auto-ignition started and a voluminous structure formed. Changes in the color and the intensity of the UC emission were observed and attributed to the monoclinic to cubic structural transformation in the Gd_2O_3 nanoparticles due to a postsynthesis heat treatment of the sample at 600°C and 900°C. The upconverting Gd_2O_3 nanopowders were found to be also useful for optical thermometry, by considering the Er^{3+} UC emission in the green region from the two thermally coupled excited states $^2H_{11/2}$ and $^4S_{3/2}$ of Er^{3+}, centered at wavelengths of 523 and 548 nm. In the 300–900 K temperature range, the maximum sensitivity derived from the fluorescence intensity ratio technique of the green UC emission is approximately 0.0039 K^{-1}.

Garnets hosts were also considered as hosts for upconverter nanomaterials. Capobianco et al. investigated Er^{3+}-doped and Tm^{3+} and Yb^{3+} codoped $Gd_3Ga_5O_{12}$ (GGG) prepared by the combustion synthesis using glycine as the fuel. This garnet host resulted to be much less prone to incorporate water and CO_2 on the particle surface with respect to sesquioxides, with great benefit to the lanthanide emission properties, increased by a less pronounced nonradiative decay due to water phonons. NIR to visible UC of the nanocrystalline Er^{3+}-doped $Gd_3Ga_5O_{12}$ was studied following excitation of the $^4I_{9/2}$ exited state upon 800 nm laser excitation (Vetrone et al. 2003). It was found that if the Er^{3+} doping is low (around 1%) ESA was the predominant mechanism responsible for populating the upper emitting states. However, as the Er^{3+} concentration was increased to 5%, the decay times for the UC emissions were lengthened and deviated from exponentiality, suggesting the presence of ETU. The 1% each Tm^{3+} and Yb^{3+} codoped $Gd_3Ga_5O_{12}$ nanostructured sample showed strong UC emission in the UV ($^1D_2 \rightarrow {}^3H_6$), blue ($^1D_2 \rightarrow {}^3F_4$), blue-green ($^1G_4 \rightarrow {}^3H_6$), red ($^1G_4 \rightarrow {}^3F_4$), and NIR ($^1G_4 \rightarrow {}^3H_5/{}^3H_4 \rightarrow {}^3H_6$) regions upon excitation of the Yb^{3+} ions with a 980 nm laser radiation (Pandozzi et al. 2005). Due to subsequent energy transfers from the Yb^{3+} ion to the Tm^{3+} ions (energy transfer efficiency about 0.576).

3.3.6 Ionic Liquids

Ionic liquids (ILs) are considered nowadays interesting materials for preparation of inorganic materials as a "green" alternative to the conventional solvents (Lorbeer et al. 2010, 2011). They have unique properties, as thermal and chemical stability, a wide electrochemical window. Moreover, ILs can act as capping agents or surfactants in the inorganic synthesis. Although ILs are very useful for nanoparticles preparation, a certain amount of agglomeration of the prepared nanoparticles is one of the main drawbacks of the technique.

In the past few years, some papers have appeared in the literature to prepare upconverting nanomaterials using the ILs technique, succeeding also

to generate various nanocrystal sizes and morphologies. Eu^{3+}-doped GdF_3 nanoparticles have been prepared by the ILs technique by Lorbeer et al. (2010) with a microwave reaction starting from the lanthanide acetates. Fast and efficient synthesis of small, uniform, oxygen-free lanthanide nanofluorides with excellent luminescence has been achieved and a quantum efficiency of up to 145% was determined. Moreover, the same group succeeded in preparing pure, oxygen-free hexagonal EuF_3 nanoparticles by reacting europium acetate hydrate with PF_6 and BF_4 ILs at 120°C using microwave synthesis, with reaction times as short as 30 s (Lorbeer et al. 2011). Extremely small particles (<15 nm) were obtained and the morphology varied from nearly spherical and cuboid to rodlike crystallites forming larger clusters. Very interestingly, the size and shape varied in different ILs. Lanthanide-doped YF_3 nanoparticles were prepared by Nuñez and coworkers using $BmimBF_4$ as the fluoride source (Nuñez and Ocaña 2007). In most cases, highly uniform NPs were obtained and their size could be varied in the nanometer range by adjusting the nature and concentration of the starting lanthanide precursors. Zhang et al. (2008) have synthesized a series of lanthanide fluoride nanocrystals in three ILs (i.e., $OmimPF_6$, $OmimBF_4$, and $BmimPF_6$), utilizing the partial hydrolysis of PF_6^- and BF_4^- to introduce a fluoride source. Lanthanum fluoride nanocrystals can be obtained in a large amount (products up to 0.15 g per 10 mL solvents) with the ILs technique. Interestingly, in these "all-in-one" systems, the ILs acted as solvents, reaction agents, and templates. Regarding different upconverting fluorides, water-soluble and pure hexagonal-phase Yb^{3+} or Er^{3+} and Tm^{3+}-doped $NaYF_4$ nanoparticles were successfully obtained by Liu et al. (2009) with use of a IL, $BmimBF_4$, which acts as solvent, template, and also fluorine source. One interesting advantage of the obtained nanocrystals is that the ILs overlayer on their surface renders them directly dispersed in water.

Spherical $NaYF_4$ nanoclusters have been synthesized using an IL (1-butyl-3-methylimidazolium tetrafluoroborate) based technique using a microwave reaction system. The nanoclusters have diameters ranging from 200 to 430 nm and are formed by the self-assembly of smaller $NaYF_4$ nanoparticles. Quite interestingly, the size of the nanoclusters could be easily controlled by variations of the precursor amounts. It was demonstrated that the ILs have key roles as solvents for the reaction, absorbents of microwave radiation, and the main fluorine sources for the $NaYF_4$ generation. The obtained nanoclusters exhibit excellent UC properties.

An interesting approach combining more synthetic techniques was introduced by He et al. (2011) to prepare lanthanide-doped upconverting $NaGdF_4$ nanocrystals with various crystalline structures. This approach used an OA/IL two-phase system that combined the advantages of the thermal decomposition and ILs techniques, exploiting the two-phase approach in the OA- and IL-phase through a one-step controllable reaction.

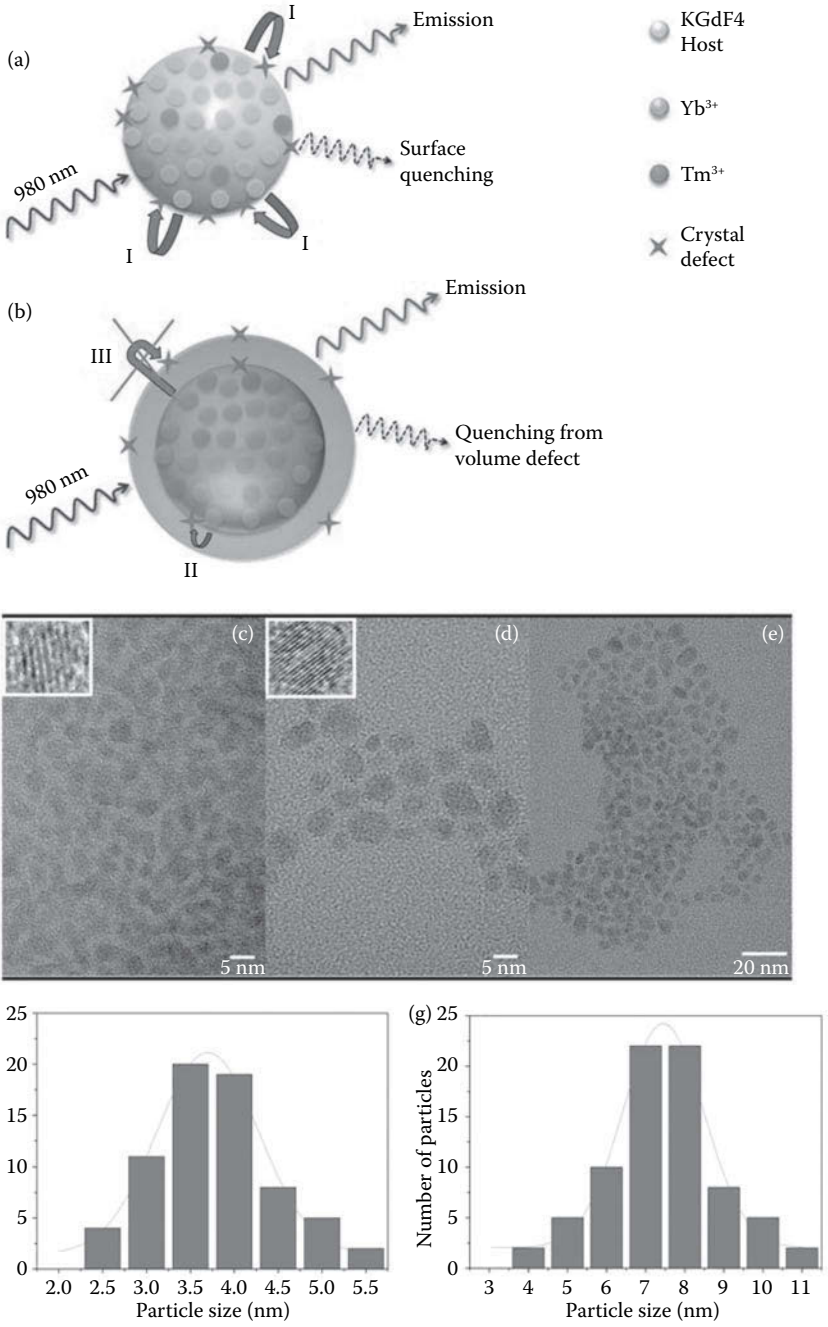

3.4 Core–Shell Architectures

"Core-only" lanthanide-doped nanoparticles, prepared with different synthetic approaches, present surface defects that are detrimental for UC emission. Moreover, lanthanide ions on the surface of nanoparticles which have been dispersed in solvents, experience an increased nonradiative multiphonon relaxation (due to the solvent phonons) with respect to those ions located in the interior of the nanoparticle. To improve the emission efficiency, a strategy is to cover the nanoparticle with an additional shell, usually with a second step procedure, using core-only nanoparticles as seeds. Quite recently, this general approach was applied by several research groups to develop NIR-to-NIR emitting nanocrystals, and can also be used to design core–shell (core@shell) nanocrystals that present fine tuning of UC emission—exploiting trapping of the migrating energy by the activators and the elimination of deleterious cross-relaxation phenomena (Wang et al. 2011). With the core@shell approach it is still possible to reach highly monodispersed nanoparticles, but some complications could arise from poorly uniform shell formation or in the purification steps, because of the self-nucleation of the shell precursors.

Capobianco et al. (Vetrone et al. 2009) synthesized hydrophobic $NaGdF_4$:Er^{3+}, Yb^{3+} active-core@$NaGdF_4$ inert-shell nanoparticles and $NaGdF_4$:Er^{3+}, Yb^{3+} active-core@$NaGdF_4$:Yb^{3+} active-shell nanoparticles (average particle size 16 nm) by a modified thermal decomposition synthesis, starting from trifluoroacetate precursors, ODE and OA. It was found that the active shell protects the active Er^{3+} ions from nonradiative decays, and efficiently transfers the incident NIR radiation to the active core. The same research group developed water dispersible ultra-small (<10 nm) multifunctional $KGdF_4$:Tm^{3+}, Yb^{3+} nanoparticles with NIR-to-NIR UC emission properties (λ_{ex} = 980 nm, λ_{em} = 803 nm), for which the luminescence efficiency was optimized with the core–shell approach. The $KGdF_4$:Tm^{3+}, Yb^{3+}@$KGdF_4$ core–shell nanoparticles were encapsulated with a PEG-phospholipid shell to obtain a water suspension (Figure 3.4) (Wong et al. 2011).

FIGURE 3.4
(a) Representation showing dopant ions in $KGdF_4$ host and the crystal defects for the core-only nanoparticles. (b) Schematization of the core–shell nanoparticles. (c) TEM image of the $KGdF_4$:Tm^{3+}, Yb^{3+} core-only nanoparticles. (d, e) TEM images of the $KGdF_4$:Tm^{3+}, Yb^{3+}@$KGdF_4$ core–shell nanoparticles showing an increase in the particles size. (f) TEM size distributions for the $KGdF_4$:Tm^{3+}, Yb^{3+} core-only nanoparticles and (g) the $KGdF_4$:Tm^{3+}, Yb^{3+}@$KGdF_4$ core–shell nanoparticles. (Wong, H.-T., F. Vetrone, R. Naccache, H. L. W. Chan, J. Hao, and J. A. Capobianco. 2011. Water dispersible ultra-small multifunctional $KGdF_4$:Tm^{3+}, Yb^{3+} nanoparticles with near-infrared to near-infrared upconversion. *J. Mater. Chem.* 21 (41):16589–16596. Reproduced by permission of The Royal Society of Chemistry.)

Small core@shell oleate-capped $NaGdF_4:Nd^{3+}@NaGdF_4$ nanocrystals (average diameter 15 nm) with efficient NIR-to-NIR downconversion PL ($\lambda_{ex} = 740$ nm, $\lambda_{em} = 850–900$ nm) were developed also by Prasad et al. for *in vitro* and *in vivo* imaging (Chen et al. 2012). They adapted a previously reported synthetic method bearing to hexagonal-phase core@shell $NaYF_4$:Yb, Tm@$NaYF_4$:Yb, Er nanocrystals containing Tm^{3+} and Er^{3+} ions in the core and in the shell, respectively. In this case, a $NaGdF_4$ shell covering a $NaGdF_4:Nd^{3+}$ core suppressed nonradiative recombination processes at the nanoparticle surface, enhancing the PL quantum yield up to 0.40.

Some of the synthetic limitations of these approaches can be by-passed using an epitaxial layer-by-layer growth of the nanocrystals, also called "self-focusing by Ostwald ripening." In this case, sacrificial nanoparticles are injected in the reaction mixture, and upon rapid dissolution (defocusing), they contribute to the formation of a uniform shell surrounding the $NaYF_4:Yb^{3+}@Er^{3+}$ core (self-focusing) (Johnson et al. 2012).

Recently, Zanzoni et al. developed a solvothermal two-step technique to prepare SrF_2 core–shell nanoparticles, in order to investigate the interaction between a protein (ubiquitin) and upconverting NPs. In this work, the $SrF_2:Yb^{3+}@SrF_2:Yb^{3+}$, Tm^{3+} core–shell architecture was adopted to ensure an efficient absorption of the NIR radiation by Yb^{3+} in both the core and shell, and to guarantee that a significant amount of emitting Tm^{3+} ions are located at the NPs surface, permitting a better investigation on the NPs–protein interaction (Zanzoni et al. 2016).

An implementation to the synthesis of lanthanide-doped NPs is based on cation exchange reactions—taking place at the nanoparticle surface—to develop multifunctional nanoprobes.

Following this scheme, a NIR-to-NIR emitting system was developed by Liu et al. (2011). The authors started from $NaYF_4:Yb^{3+}$, Er^{3+} oleate-capped nanoparticles obtained by solvothermal synthesis, to develop multifunctional upconversion nanoparticles ($NaYF_4:Yb^{3+}$, Er^{3+}), combining magnetic (Gd^{3+}), positron emission tomography (PET) (^{18}F), and targeted recognition (FA) properties (Figure 3.5). In particular, Gd^{3+} ions were introduced on the surface of the nanocrystals by cation exchange with Y^{3+} ions, while ^{18}F was introduced for PET imaging by interaction with the RE ions.

In a related example, Van Veggel et al. performed cation exchange with Gd^{3+} ions on upconverting $NaYF_4:Yb^{3+}$, Tm^{3+} nanoparticles (Dong et al. 2012). They started from oleate-stabilized $NaYF_4:Yb^{3+}$, Tm^{3+} nanoparticles (average diameter 19–20 nm) synthesized using a coprecipitation method in organic media at 300°C (Figure 3.6).

Ligand exchange of the as-prepared oleate-stabilized nanoparticles with PVP (Johnson et al. 2010) provided a water dispersible system that was exposed to Gd^{3+} to obtain the bimodal $NaYF_4:Yb^{3+}$, Tm@$NaGdF_4$ core@shell nanoparticles. The sub-nanometer $NaGdF_4$ shell (ca. 0.6 nm) conferred very high proton relaxivity to the nanoparticle for targeted MRI applications.

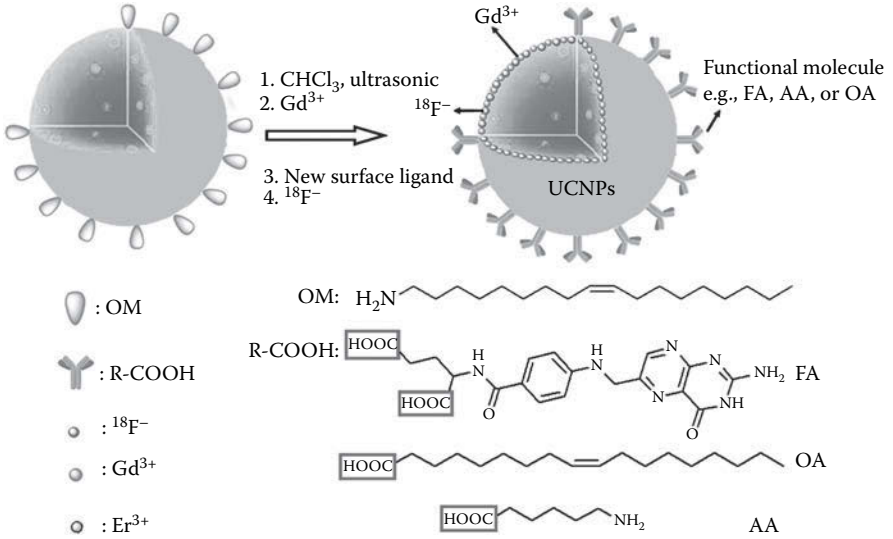

FIGURE 3.5
Schematic representation of ^{18}F-labeled magnetic-UC functional nanocrystals. OM: oleyl amine; FA: folic acid; OA: oleic acid; and AA: aminocaproic acid. (Reprinted with permission from Liu, Q., Y. Sun, C. Li, J. Zhou, C. Li, T. Yang, X. Zhang, T. Yi, D. Wu, and F. Li. 2011. F-18-labeled magnetic-upconversion nanophosphors via rare-earth cation-assisted ligand assembly. *ACS Nano* 5 (4):3146–3157. Copyright 2011 American Chemical Society.)

3.4.1 Silica-Shell Formation

Nanoparticles tailored for biological imaging applications need to provide stable suspension in water and buffered solutions, and often the possibility to introduce chemical functionalities for biomolecule targeting. Most of the "as-prepared" lanthanide-doped nanoparticles are capped with hydrophobic molecules such as oleate (Li et al. 2008) or OM (Chan et al. 2012), and for this reason, several approaches were developed to increase the polarity of the nanoparticle surface to obtain water dispersibility. An overview of these synthetic approaches has been recently reviewed in focused publications (Muhr et al. 2014; Sedlmeier and Gorris 2014). Silica encapsulation offers the possibility to endow lanthanide-doped nanocrystals with a surface material that is hydrophilic, transparent to radiation and photophysically inert, simple to functionalize, and intrinsically nontoxic (Arap et al. 2013; Bonacchi et al. 2011; Genovese et al. 2014). The shell usually does not affect the emission efficiency of the nanocrystals, and actually in some cases improves it. Beside this behavior, silica can be independently doped with other fluorophores or contrast agents (Qian et al. 2009), or drugs to develop multimodal imaging or theranostic tools: this possibility is fostered by mesoporous silica shells (Li et al. 2013; P. Yang et al. 2012), formed

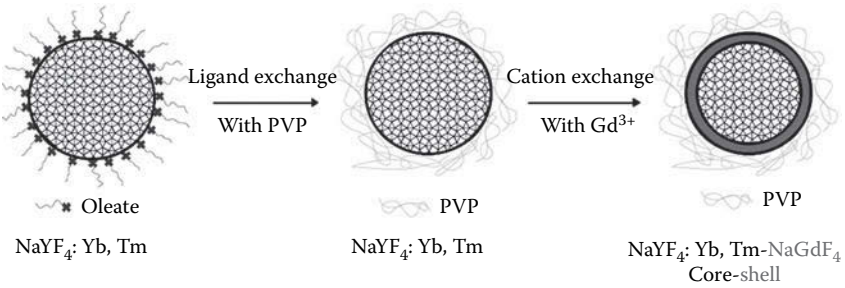

FIGURE 3.6
Schematization of the cation exchange process to form $NaYF_4$:Yb, Tm@$NaGdF_4$ core–shell nanoparticles. (Dong, C., A. Korinek, B. Blasiak, B. Tomanek, and F. C. J. M. van Veggel. 2012. Cation exchange: A facile method to make $NaYF_4$:Yb^{3+}, Tm^{3+}@$NaGdF_4$ core@shell nanoparticles with a thin, tunable, and uniform shell. *Chem. Mater.* 24 (7):1297–1305. Reproduced by permission of The Royal Society of Chemistry.)

adding to the synthetic mixture surfactant agents like CTAB (Liu et al. 2012; Qian et al. 2009).

A few synthetic approaches are available to cover lanthanides-doped nanosystems: nanoparticles presenting hydrophobic capping agents are frequently coated using a reverse microemulsion approach (water-in-oil) (Jalil and Zhang 2008). Silica coating involves an increase of the nanoparticles average diameter, a process that may cause some loss of monodispersity of the starting material: for this reason, most of the reports adopt this approach, starting from very monodisperse OA-capped nanocrystals and using the microemulsion method for silica shell formation, that guarantees nanocrystals core confinement within the reverse micelles of the microemulsion (Li et al. 2008). Shell thickness can be varied mainly acting on the amount of tetrathoxysilane introduced in the microemulsion and/or on the surfactant-to-water ratio, the main parameter affecting the number of reverse micelles within the microemulsion.

In a recent example, Li et al. (Zhu et al. 2014) developed a NIR-to-NIR emitting imaging (Figure 3.7).

Lanthanide-doped core was synthesized by a solvothermal method (average diameter 20 nm), and during the silica coating step ethoxysilane functionalized PEG (PEG–siloxane) was added into the microemulsion to achieve PEGylation (final hydrodynamic diameter ~65 nm).

Hydrophilic nanocrystals are usually coated in water–alcohol mixtures using a Stöber approach (Stöber et al. 1968). With this strategy, Wolfbeis et al. (Mader et al. 2010) faced the coating of lanthanide-doped nanoparticles and microparticles with average diameters spanning from 50 nm to 15 μm. They adopted a click chemistry-based strategy to functionalize the surface of the nano- and microparticles with a few "click reagents" and alkyne-modified fluorescent dyes.

FIGURE 3.7
TEM images of (a) $NaYF_4$:Yb, Tm UCNPs and (b) $NaYF_4$:Yb^{3+}, Tm^{3+}@SiO_2 nanoparticles modified with PEG (PEG-UCNPs), and room temperature UCL spectrum of PEG-UCNPs in water (5 mg/mL, λ_{ex} = 980 nm). (Zhu, X., B. Da Silva, X. Zou, B. Shen, Y. Sun, W. Feng, and F. Li. 2014. Intra-arterial infusion of PEGylated upconversion nanophosphors to improve the initial uptake by tumors *in vivo*. *RSC Adv.* 4 (45):23580–23584. Reproduced by permission of The Royal Society of Chemistry.)

The silica modification quite often produces systems that are prone to aggregation processes and unspecific binding, and for this reason just the formation of an ultrathin silica shell of few nanometers (Li and Zhang 2006; F. Liu et al. 2013) or proper functionalization treatments (Bagwe et al. 2006) were developed.

Polymer-coated lanthanide-doped nanoparticles can also be coated by a silica shell, since some polymers such as PVP (Li and Zhang 2006) favor the condensation of a silica layer. This approach moves toward more direct coating protocols since PVP is often used as a stabilizing agents in many hydrothermal syntheses. Surface modification can be carried out during the growth of the silica shell or after its formation, and besides colloidal stabilization endow nanoparticles with moieties bearing $–NH_2$ (M. Wang et al. 2009), –COOH (F. Liu et al. 2013), –SH (Y. Yang et al. 2012), or functional groups for click chemistry (Mader et al. 2010).

3.5 Conclusions

Despite the great attention devoted to UCNPs presenting unique optical and chemical properties, their practical application is still limited. This is mainly due to a few demanding features including their nontrivial and, sometimes, poorly reproducible synthetic procedures. In this chapter, we have summarized the recent achievements in the development of more and more efficient preparation methods, with emphasis on the pros and cons of each strategy (Table 3.1). Presently, with a careful control and tuning of the reaction conditions, it is possible to obtain monodispersed and customized UCNPs with many different components. It has to be underlined, however, that the quantum yield of these materials is still generally not very high and it dramatically depends not only on the components but also on the architecture of the nanoparticle (local environment around the lanthanide ions and structure). Consequently, the research on new and optimized synthetic and surface modification methods is a fundamental step toward the application of these species. Great efforts are now devoted to investigate nondemanding and reproducible approaches for large-scale preparations of multifunctional, multi-shell UCNPs able to fulfill practical needs.

References

Abel, K. A., J.-C. Boyer, and F. C. J. M. van Veggel. 2009. Hard proof of the $NaYF_4$/$NaGdF_4$ nanocrystal core/shell structure. *J. Am. Chem. Soc.* 131 (41):14644–14645.

Arap, W., R. Pasqualini, M. Montalti, L. Petrizza, L. Prodi, E. Rampazzo, N. Zaccheroni, and S. Marchio. 2013. Luminescent silica nanoparticles for cancer diagnosis. *Curr. Med. Chem.* 20 (17):2195–2211.

Auzel, F. 2004. Upconversion and anti-Stokes processes with f and d ions in solids. *Chem. Rev.* 104 (1):139–173.

Bagwe, R. P., L. R. Hilliard, and W. Tan. 2006. Surface modification of silica nanoparticles to reduce aggregation and nonspecific binding. *Langmuir* 22 (9):4357–4362.

Bonacchi, S., D. Genovese, R. Juris, M. Montalti, L. Prodi, E. Rampazzo, and N. Zaccheroni. 2011. Luminescent silica nanoparticles: Extending the frontiers of brightness. *Angew. Chem. Int. Ed.* 50 (18):4056–4066.

Boyer, J. C., J. Gagnon, L. A. Cuccia, and J. A. Capobianco. 2007. Synthesis, characterization, and spectroscopy of $NaGdF_4$: Ce^{3+}, $Tb^{3+}/NaYF_4$ core/shell nanoparticles. *Chem. Mater.* 19 (14):3358–3360.

Boyer, J.-C., F. Vetrone, L. A. Cuccia, and J. A. Capobianco. 2006. Synthesis of colloidal upconverting $NaYF_4$ nanocrystals doped with Er^{3+}, Yb^{3+} and Tm^{3+}, Yb^{3+} via thermal decomposition of lanthanide trifluoroacetate precursors. *J. Am. Chem. Soc.* 128 (23):7444–7445.

Cao, T. Y., Y. Yang, Y. A. Gao, J. Zhou, Z. Q. Li, and F. Y. Li. 2011. High-quality water-soluble and surface-functionalized upconversion nanocrystals as luminescent probes for bioimaging. *Biomaterials* 32 (11):2959–2968.

Cao, Y. C. 2004. Synthesis of square gadolinium-oxide nanoplates. *J. Am. Chem. Soc.* 126 (24):7456–7457.

Capobianco, J. A., F. Vetrone, T. D'Alesio, G. Tessari, A. Speghini, and M. Bettinelli. 2000. Optical spectroscopy of nanocrystalline cubic Y_2O_3:Er^{3+} obtained by combustion synthesis. *Phys. Chem. Chem. Phys.* 2 (14):3203–3207.

Chan, E. M., G. Han, J. D. Goldberg, D. J. Gargas, A. D. Ostrowski, P. J. Schuck, B. C. Cohen, and D. J. Milliron. 2012. Combinatorial discovery of lanthanide-doped nanocrystals with spectrally pure upconverted emission. *Nano Lett.* 12:3839–3845.

Chen, D., Y. Yu, F. Huang, P. Huang, A. Yang, and Y. Wang. 2010. Modifying the size and shape of monodisperse bifunctional alkaline-earth fluoride nanocrystals through lanthanide doping. *J. Am. Chem. Soc.* 132 (29):9976–9978.

Chen, G., T. Y. Ohulchanskyy, R. Kumar, H. Agren, and P. N. Prasad. 2010. Ultrasmall monodisperse $NaYF_4$:Yb^{3+}/Tm^{3+} nanocrystals with enhanced near-infrared to near-infrared upconversion photoluminescence. *ACS Nano* 4 (6):3163–3168.

Chen, G., H. Qiu, P. N. Prasad, and X. Chen. 2014. Upconversion nanoparticles: Design, nanochemistry, and applications in theranostics. *Chem. Rev.* 114 (10):5161–5214.

Chen, G., C. Yang, and P. N. Prasad. 2013. Nanophotonics and nanochemistry: Controlling the excitation dynamics for frequency up- and down-conversion in lanthanide-doped nanoparticles. *Acc. Chem. Res.* 46 (7):1474–1486.

Chen, G. Y., T. Y. Ohulchanskyy, S. Liu, W. C. Law, F. Wu, M. T. Swihart, H. Agren, and P. N. Prasad. 2012. Core/shell $NaGdF_4$:$Nd^{3+}/NaGdF_4$ nanocrystals with efficient near-infrared to near-infrared downconversion photoluminescence for bioimaging applications. *ACS Nano* 6 (4):2969–2977.

Cichos, J., L. Marciniak, D. Hreniak, W. Strek, and M. Karbowiak. 2014. The effect of surface ligand, solvent and Yb^{3+} co-doping on the luminescence properties of Er^{3+} in colloidal $NaGdF_4$ nanocrystals. *J. Mater. Chem. C* 2 (39):8244–8251.

Cuccia, L. A. and J. A. Capobianco. 2007. Synthesis of colloidal upconverting $NaYF_4$: Er^{3+}/Yb^{3+} and Tm^{3+}/Yb^{3+} monodisperse nanocrystals. *Nano Lett*. 7 (3):847–852.

DaCosta, M. V., S. Doughan, Y. Han, and U. J. Krull. 2014. Lanthanide upconversion nanoparticles and applications in bioassays and bioimaging: A review. *Anal. Chim. Acta* 832:1–33.

Daldosso, M., D. Falcomer, A. Speghini, M. Bettinelli, S. Enzo, B. Lasio, and S. Polizzi. 2008. Synthesis, structural investigation and luminescence spectroscopy of nanocrystalline $Gd_3Ga_5O_{12}$ doped with lanthanide ions. *J. Alloy. Compd.* 451 (1–2):553–556.

De la Rosa-Cruz, E., L. A. Diaz-Torres, R. A. Rodriguez-Rojas, M. A. Meneses-Nava, O. Barbosa-Garcia, and P. Salas. 2003. Luminescence and visible upconversion in nanocrystalline ZrO_2:Er^{3+}. *Appl. Phys. Lett.* 83 (24):4903–4905.

Dong, C., A. Korinek, B. Blasiak, B. Tomanek, and F. C. J. M. van Veggel. 2012. Cation exchange: A facile method to make $NaYF_4$:Yb, Tm-$NaGdF_4$ core–shell nanoparticles with a thin, tunable, and uniform shell. *Chem. Mater.* 24 (7):1297–1305.

Dorman, J. A., J. H. Choi, G. Kuzmanich, and J. P. Chang. 2012. Elucidating the effects of a rare-earth oxide shell on the luminescence dynamics of Er^{3+}:Y_2O_3 nanoparticles. *J. Phys. Chem. C* 116 (18):10333–10340.

Du, Y.-P., X. Sun, Y.-W. Zhang, Z.-G. Yan, L.-D. Sun, and C.-H. Yan. 2009. Uniform alkaline earth fluoride nanocrystals with diverse shapes grown from thermolysis of metal trifluoroacetates in hot surfactant solutions. *Cryst. Growth Des.* 9 (4):2013–2019.

Du, Y.-P., Y.-W. Zhang, L.-D. Sun, and C.-H. Yan. 2008. Luminescent monodisperse nanocrystals of lanthanide oxyfluorides synthesized from trifluoroacetate precursors in high-boiling solvents. *J. Phys. Chem. C* 112 (2):405–415.

Gainer, C. F. and M. Romanowski. 2014. A review of synthetic methods for the production of upconverting lanthanide nanoparticles. *J. Innov. Opt. Heal. Sci.* 07 (02):1330007.

Genovese, D., E. Rampazzo, S. Bonacchi, M. Montalti, N. Zaccheroni, and L. Prodi. 2014. Energy transfer processes in dye-doped nanostructures yield cooperative and versatile fluorescent probes. *Nanoscale* 6 (6):3022–3036.

Guo, H., N. Dong, M. Yin, W. P. Zhang, L. R. Lou, and S. D. Xia. 2004. Visible upconversion in rare earth ion-doped Gd_2O_3 nanocrystals. *J. Phys. Chem. B* 108 (50):19205–19209.

Guo, L., Y. Wang, Y. Wang, J. Zhang, P. Dong, and W. Zeng. 2013. Structure, enhancement and white luminescence of multifunctional $Lu_6O_5F_8$:20%Yb^{3+}, 1%Er^{3+}(Tm^{3+}) nanoparticles via further doping with Li^+ under different excitation sources. *Nanoscale* 5 (6):2491–2504.

He, M., P. Huang, C. Zhang, H. Hu, C. Bao, G. Gao, R. He, and D. Cui. 2011. Dual phase-controlled synthesis of uniform lanthanide-doped $NaGdF_4$ upconversion nanocrystals via an OA/ionic liquid two-phase system for *in vivo* dual-modality imaging. *Adv. Funct. Mater.* 21 (23):4470–4477.

Heer, S., K. Kömpe, H. U. Gudel, and M. Haase. 2004. Highly efficient multicolour upconversion emission in transparent colloids of lanthanide-doped $NaYF_4$ nanocrystals. *Adv. Mater.* 16 (23–24):2102–2105.

Heer, S., O. Lehmann, M. Haase, and H. U. Gudel. 2003. Blue, green, and red upconversion emission from lanthanide-doped $LuPO_4$ and $YbPO_4$ nanocrystals in a transparent colloidal solution. *Angew. Chem. Int. Ed.* 42 (27):3179–3182.

Hemmer, E., N. Venkatachalam, H. Hyodo, A. Hattori, Y. Ebina, H. Kishimoto, and K. Soga. 2013. Upconverting and NIR emitting rare earth based nanostructures for NIR-bioimaging. *Nanoscale* 5 (23):11339–11361.

Ivaturi, A., S. K. W. MacDougall, R. Martín-Rodríguez, M. Quintanilla, J. Marques-Hueso, K. W. Krämer, A. Meijerink, and B. S. Richards. 2013. Optimizing infrared to near infrared upconversion quantum yield of β-$NaYF_4$:Er^{3+} in fluoropolymer matrix for photovoltaic devices. *J. Appl. Phys.* 114 (1):013505.

Jalil, R. A. and Y. Zhang. 2008. Biocompatibility of silica coated $NaYF_4$ upconversion fluorescent nanocrystals. *Biomaterials* 29:4122–4128.

Jiang, T., W. Qin, W. Di, R. Yang, D. Liu, X. Zhai, and G. Qin. 2012. Citric acid-assisted hydrothermal synthesis of α-$NaYF_4$:Yb^{3+}, Tm^{3+} nanocrystals and their enhanced ultraviolet upconversion emissions. *CrystEngComm* 14 (6):2302–2307.

Johnson, N. J. J., A. Korinek, C. Dong, and F. C. J. M. van Veggel. 2012. Self-focusing by Ostwald ripening: A strategy for layer-by-layer epitaxial growth on upconverting nanocrystals. *J. Am. Chem. Soc.* 134 (27):11068–11071.

Johnson, N. J. J., W. Oakden, G. J. Stanisz, R. Scott Prosser, and F. C. J. M. van Veggel. 2011. Size-tunable, ultra small $NaGdF_4$ nanoparticles: Insights into their T1 MRI contrast enhancement. *Chem. Mater.* 23 (16):3714–3722.

Johnson, N. J. J., N. M. Sangeetha, J.-C. Boyer, and F. C. J. M. van Veggel. 2010. Facile ligand-exchange with polyvinylpyrrolidone and subsequent silica coating of hydrophobic upconverting [small beta]-$NaYF_4$:Yb^{3+}/Er^{3+} nanoparticles. *Nanoscale* 2 (5):771–777.

Krämer, K. W., D. Biner, G. Frei, H. U. Güdel, M. P. Hehlen, and S. R. Lüthi. 2004. Hexagonal sodium yttrium fluoride based green and blue emitting upconversion phosphors. *Chem. Mater.* 16 (7):1244–1251.

Li, C., Z. Hou, Y. Dai, D. Yang, Z. Cheng, P. Ma, and J. A. Lin. 2013. A facile fabrication of upconversion luminescent and mesoporous core–shell structured β-$NaYF_4$:Yb^{3+}, Er^{3+}@$mSiO_2$ nanocomposite spheres for anti-cancer drug delivery and cell imaging. *Biomater. Sci.* 1:213–223.

Li, Z. and Y. Zhang. 2006. Monodisperse silica-coated polyvinylpyrrolidone/$NaYF_4$ nanocrystals with multicolor upconversion fluorescence emission. *Angew. Chem. Int. Ed.* 45 (46):7732–7735.

Li, Z. and Y. Zhang. 2008. An efficient and user-friendly method for the synthesis of hexagonal-phase $NaYF_4$: Yb, Er/Tm nanocrystals with controllable shape and upconversion fluorescence. *Nanotechnology* 19 (34):345606.

Li, Z., Y. Zhang, and S. Jiang. 2008. Multicolor core/shell-structured upconversion fluorescent nanoparticles. *Adv. Mater.* 20 (24):4765–4769.

Lin, M., Y. Zhao, M. Liu, M. S. Qiu, Y. Q. Dong, Z. F. Duan, Y. H. Li, B. Pingguan-Murphy, T. J. Lu, and F. Xu. 2014. Synthesis of upconversion $NaYF_4$:Yb^{3+}, Er^{3+} particles with enhanced luminescent intensity through control of morphology and phase. *J. Mater. Chem. C* 2 (19):3671–3676.

Liu, F., Q. Zhao, H. You, and Z. Wang. 2013. Synthesis of stable carboxy-terminated $NaYF_4$: Yb^{3+}, Er^{3+}@SiO_2 nanoparticles with ultrathin shell for biolabeling applications. *Nanoscale* 5 (3):1047–1053.

Liu, J., W. Bu, S. Zhang, F. Chen, H. Xing, L. Pan, L. Zhou, W. Peng, and J. Shi. 2012. Controlled synthesis of uniform and monodisperse upconversion core/mesoporous silica shell nanocomposites for bimodal imaging. *Chem. Eur. J.* 18 (8):2335–2341.

Liu, Q., Y. Sun, C. Li, J. Zhou, C. Li, T. Yang, X. Zhang, T. Yi, D. Wu, and F. Li. 2011. F-18-labeled magnetic-upconversion nanophosphors via rare-earth cation-assisted ligand assembly. *ACS Nano* 5 (4):3146–3157.

Liu, X. M., J. W. Zhao, Y. J. Sun, K. Song, Y. Yu, C. A. Du, X. G. Kong, and H. Zhang. 2009. Ionothermal synthesis of hexagonal-phase $NaYF_4$:Yb^{3+}, Er^{3+}/Tm^{3+} upconversion nanophosphors. *Chem. Commun.* 6628–6630.

Liu, Y., D. Tu, H. Zhu, and X. Chen. 2013. Lanthanide-doped luminescent nanoprobes: Controlled synthesis, optical spectroscopy, and bioapplications. *Chem. Soc. Rev.* 42:6924–6958.

Liu, Y., D. Tu, H. Zhu, R. Li, W. Luo, and X. Chen. 2010. A strategy to achieve efficient dual-mode luminescence of Eu^{3+} in lanthanides doped multifunctional $NaGdF_4$ nanocrystals. *Adv. Mater.* 22 (30):3266–3271.

Liu, Z., F. Pu, S. Huang, Q. Yuan, J. Ren, and X. Qu. 2013. Long-circulating Gd_2O_3:Yb^{3+}, Er^{3+} up-conversion nanoprobes as high-performance contrast agents for multimodality imaging. *Biomaterials* 34 (6):1712–1721.

Lorbeer, C., J. Cybińska, and A.-V. Mudring. 2010. Facile preparation of quantum cutting GdF_3:Eu^{3+} nanoparticles from ionic liquids. *Chem. Commun. (Cambridge, England)* 46 (4):571–573.

Lorbeer, C., J. Cybińska, and A.-V. Mudring. 2011. Europium(III) fluoride nanoparticles from ionic liquids: Structural, morphological, and luminescent properties. *Cryst. Growth Des.* 11 (4):1040–1048.

Lu, Q., F. Y. Guo, L. Sun, A. H. Li, and L. C. Zhao. 2008. Silica-/titania-coated Y_2O_3: Tm^{3+}, Yb^{3+} nanoparticles with improvement in upconversion luminescence induced by different thickness shells. *J. Appl. Phys.* 103 (12):123533.

Lu, Q. P., Y. B. Hou, A. W. Tang, Y. Z. Lu, L. F. Lv, and F. Teng. 2014. Controlled synthesis and defect dependent upconversion luminescence of Y_2O_3: Yb, Er nanoparticles. *J. Appl. Phys.* 115 (7):074309.

Luo, W. Q., C. Y. Fu, R. F. Li, Y. S. Liu, H. M. Zhu, and X. Y. Chen. 2011. Er^{3+}-doped anatase TiO_2 nanocrystals: Crystal-field levels, excited-state dynamics, upconversion, and defect luminescence. *Small* 7 (21):3046–3056.

Lv, R., S. Gai, Y. Dai, N. Niu, F. He, and P. Yang. 2013. Highly uniform hollow GdF_3 spheres: Controllable synthesis, tuned luminescence, and drug-release properties. *ACS Appl. Mater. Inter.* 5 (21):10806–10818.

Mader, H. S., M. Link, D. E. Achatz, K. Uhlmann, X. Li, and O. S. Wolfbeis. 2010. Surface-modified upconverting microparticles and nanoparticles for use in click chemistries. *Chem. Eur. J.* 16 (18):5416–5424.

Mai, H. X., Y. W. Zhang, R. Si, Z. G. Yan, L. Sun, L. P. You, and C. H. Yan. 2006. High-quality sodium rare-earth fluoride nanocrystals: Controlled synthesis and optical properties. *J. Am. Chem. Soc.* 128 (19):6426–6436.

Mita, Y., H. Yamamoto, K. Katayanagi, and S. Shionoya. 1995. Energy transfer processes in Er^{3+}- and Yb^{3+}-doped infrared upconversion materials. *J. Appl. Phys.* 78 (2):1219–1223.

Muhr, V., S. Wilhelm, T. Hirsch, and O. S. Wolfbeis. 2014. Upconversion nanoparticles: From hydrophobic to hydrophilic surfaces. *Acc. Chem. Res.* 47 (12):3481–3493.

Naccache, R., F. Vetrone, V. Mahalingam, L. A. Cuccia, and J. A. Capobianco. 2009. Controlled synthesis and water dispersibility of hexagonal phase $NaGdF_4$:Ho^{3+}/Yb^{3+} nanoparticles. *Chem. Mater.* 21 (4):717–723.

Nguyen, T. D., C. T. Dinh, and T. O. Do. 2010. Shape- and size-controlled synthesis of monoclinic ErOOH and cubic Er_2O_3 from micro- to nanostructures and their upconversion luminescence. *ACS Nano* 4 (4):2263–2273.

Nuñez, N. O. and M. Ocaña. 2007. An ionic liquid based synthesis method for uniform luminescent lanthanide fluoride nanoparticles. *Nanotechnology* 18 (45):455606.

Pandozzi, F., F. Vetrone, J. C. Boyer, R. Naccache, J. A. Capobianco, A. Speghini, and M. Bettinelli. 2005. A spectroscopic analysis of blue and ultraviolet upconverted emissions from $Gd_3Ga_5O_{12}$:Tm^{3+}, Yb^{3+} nanocrystals. *J. Phys. Chem. B* 109 (37):17400–17405.

Passuello, T., M. Pedroni, F. Piccinelli et al. 2012. PEG-capped, lanthanide doped GdF_3 nanoparticles: Luminescent and T_2 contrast agents for optical and MRI multimodal imaging. *Nanoscale* 4 (24):7682–7689.

Passuello, T., F. Piccinelli, M. Pedroni, M. Bettinelli, F. Mangiarini, R. Naccache, F. Vetrone, J. A. Capobianco, and A. Speghini. 2011a. White light upconversion of nanocrystalline Er/Tm/Yb doped tetragonal $Gd_4O_3F_6$. *Opt. Mater.* 33 (4):643–646.

Passuello, T., F. Piccinelli, M. Pedroni, S. Polizzi, F. Mangiarini, F. Vetrone, M. Bettinelli, and A. Speghini. 2011b. NIR-to-visible and NIR-to-NIR upconversion in lanthanide doped nanocrystalline GdOF with trigonal structure. *Opt. Mater.* 33 (10):1500–1505.

Patra, A., C. S. Friend, R. Kapoor, and P. N. Prasad. 2002. Upconversion in Er^{3+}:ZrO_2 nanocrystals. *J. Phys. Chem. B* 106 (8):1909–1912.

Patra, A., C. S. Friend, R. Kapoor, and P. N. Prasad. 2003a. Effect of crystal nature on upconversion luminescence in Er^{3+}:ZrO_2 nanocrystals. *Appl. Phys. Lett.* 83 (2):284.

Patra, A., C. S. Friend, R. Kapoor, and P. N. Prasad. 2003b. Fluorescence upconversion properties of Er^{3+}-doped TiO_2 and $BaTiO_3$ nanocrystallites. *Chem. Mater.* 15 (19):3650–3655.

Peacock, R. D. 1975. The intensities of lanthanide f–f transitions. *Struct. Bond.* 22:83–122.

Pedroni, M., F. Piccinelli, T. Passuello, M. Giarola, G. Mariotto, S. Polizzi, M. Bettinelli, and A. Speghini. 2011. Lanthanide doped upconverting colloidal CaF_2 nanoparticles prepared by a single-step hydrothermal method: Toward efficient materials with near infrared-to-near infrared upconversion emission. *Nanoscale* 3 (4):1456–1460.

Pedroni, M., F. Piccinelli, T. Passuello et al. 2013. Water (H_2O and D_2O) dispersible NIR-to-NIR upconverting Yb^{3+}/Tm^{3+} doped MF_2 (M = Ca, Sr) colloids: Influence of the host crystal. *Cryst. Growth Des.* 13 (11):4906–4913.

Pedroni, M., F. Piccinelli, S. Polizzi, A. Speghini, M. Bettinelli, and P. Haro-González. 2012. Upconverting Ho–Yb doped titanate nanotubes. *Mater. Lett.* 80:81–83.

Polizzi, S., S. Bucella, A. Speghini, F. Vetrone, R. Naccache, J. C. Boyer, and J. A. Capobianco. 2004. Nanostructured lanthanide-doped Lu_2O_3 obtained by propellant synthesis. *Chem. Mater.* 16 (7):1330–1335.

Polizzi, S., G. Fagherazzi, M. Battagliarin, M. Bettinelli, and A. Speghini. 2001. Fractal aggregates of lanthanide-doped Y_2O_3 nanoparticles obtained by propellant synthesis. *J. Mater. Res.* 16 (1):146–154.

Prodi, L., E. Rampazzo, F. Rastrelli, A. Speghini, and N. Zaccheroni. 2015. Imaging agents based on lanthanide doped nanoparticles. *Chem. Soc. Rev.* 44 (14):4922–4952.

Qian, H. S., H. C. Guo, P. C.-L. Ho, R. Mahendran, and Y. Zhang. 2009. Mesoporous-silica-coated up-conversion fluorescent nanoparticles for photodynamic therapy. *Small* 5 (20):2285–2290.

Quan, Z., D. Yang, P. Yang, X. Zhang, H. Lian, X. Liu, and J. Lin. 2008. Uniform colloidal alkaline earth metal fluoride nanocrystals: Nonhydrolytic synthesis and luminescence properties. *Inorg. Chem.* 47 (20):9509–9517.

Schafer, H., P. Ptacek, H. Eickmeier, and M. Haase. 2009. Synthesis of hexagonal Yb^{3+}, Er^{3+}-doped $NaYF_4$ nanocrystals at low temperature. *Adv. Funct. Mater.* 19 (19):3091–3097.

Sedlmeier, A. and H. H. Gorris. 2014. Surface modification and characterization of photon-upconverting nanoparticles for bioanalytical applications. *Chem. Soc. Rev.* 44:1526–1560.

Si, R., Y. W. Zhang, H. P. Zhou, L. D. Sun, and C. H. Yan. 2007. Controlled-synthesis, self-assembly behavior, and surface-dependent optical properties of high-quality rare-earth oxide nanocrystals. *Chem. Mater.* 19 (1):18–27.

Singh, S. K., K. Kumar, and S. B. Rai. 2008. Multifunctional Er^{3+}–Yb^{3+} codoped Gd_2O_3 nanocrystalline phosphor synthesized through optimized combustion route. *Appl. Phys. B* 94 (1):165–173.

Singh, S. K., K. Kumar, and S. B. Rai. 2009. Er^{3+}/Yb^{3+} codoped Gd_2O_3 nano-phosphor for optical thermometry. *Sensor. Actuat. A Phys.* 149 (1):16–20.

Stöber, W., A. Fink, and E. Bohn. 1968. Controlled growth of monodisperse silica spheres in the micron size range. *J. Colloid Interf. Sci.* 26 (1):62–69.

Stouwdam, J. W. and F. C. J. M. van Veggel. 2002. Near-infrared emission of redispersible Er^{3+}, Nd^{3+}, and Ho^{3+} doped LaF_3 nanoparticles. *Nano Lett.* 2 (7):733–737.

Sun, L. D., Y. F. Wang, and C. H. Yan. 2014. Paradigms and challenges for bioapplication of rare earth upconversion luminescent nanoparticles: Small size and tunable emission/excitation spectra. *Acc. Chem. Res.* 47:1001–1009.

Sun, X., Y.-W. Zhang, Y.-P. Du, Z.-G. Yan, R. Si, L.-P. You, and C.-H. Yan. 2007. From trifluoroacetate complex precursors to monodisperse rare-earth fluoride and oxyfluoride nanocrystals with diverse shapes through controlled fluorination in solution phase. *Chem. Eur. J.* 13 (8):2320–2332.

Tian, Y., H. Y. Yang, S. S. Yu, and X. Li. 2014. Shape-controlled synthesis of monodispersed ultrasmall $CaGd_3F_{11}$ nanocrystals for potential dual-modal probes. *ChemPlusChem* 79 (11):1584–1589.

van Veggel, F. C. J. M., C. Dong, N. J. J. Johnson, and J. Pichaandi. 2012. Ln^{3+}-doped nanoparticles for upconversion and magnetic resonance imaging: Some critical notes on recent progress and some aspects to be considered. *Nanoscale* 4 (23):7309–7321.

Venkatramu, V., M. Giarola, G. Mariotto, S. Enzo, S. Polizzi, C. K. Jayasankar, F. Piccinelli, M. Bettinelli, and A. Speghini. 2010. Nanocrystalline lanthanide-doped $Lu_3Ga_5O_{12}$ garnets: Interesting materials for light-emitting devices. *Nanotechnology* 21 (17):175703.

Vetrone, F., J. C. Boyer, J. A. Capobianco, A. Speghini, and M. Bettinelli. 2003. Luminescence spectroscopy and near-infrared to visible upconversion of nanocrystalline $Gd_3Ga_5O_{12}$:Er^{3+}. *J. Phys. Chem. B* 107 (39):10747–10752.

Vetrone, F., J. C. Boyer, J. A. Capobianco, A. Speghini, and M. Bettinelli. 2004. A spectroscopic investigation of trivalent lanthanide doped Y_2O_3 nanocrystals. *Nanotechnology* 15 (1):75–81.

Vetrone, F., R. Naccache, V. Mahalingam, C. G. Morgan, and J. A. Capobianco. 2009. The active-core/active-shell approach: A strategy to enhance the upconversion luminescence in lanthanide-doped nanoparticles. *Adv. Funct. Mater.* 19 (18):2924–2929.

Wang, F., R. R. Deng, J. Wang, Q. X. Wang, Y. Han, H. M. Zhu, X. Y. Chen, and X. G. Liu. 2011. Tuning upconversion through energy migration in core–shell nanoparticles. *Nat. Mater.* 10 (12):968–973.

Wang, F., Y. Han, C. S. Lim, Y. Lu, J. Wang, J. Xu, H. Chen, C. Zhang, M. Hong, and X. Liu. 2010. Simultaneous phase and size control of upconversion nanocrystals through lanthanide doping. *Nature* 463 (7284):1061–1065.

Wang, F. and X. Liu. 2009. Recent advances in the chemistry of lanthanide-doped upconversion nanocrystals. *Chem. Soc. Rev.* 38 (4):976–989.

Wang, G., Q. Peng, and Y. Li. 2009. Upconversion luminescence of monodisperse CaF_2:Yb^{3+}/Er^{3+} nanocrystals. *J. Am. Chem. Soc.* 131 (40):14200–14201.

Wang, H., M. Uehara, H. Nakamura, M. Miyazaki, and H. Maeda. 2005. Synthesis of well-dispersed Y_2O_3:Eu nanocrystals and self-assembled nanodisks using a simple non-hydrolytic route. *Adv. Mater.* 17 (20):2506–2509.

Wang, M., C. Mi, Y. Zhang, J. Liu, F. Li, C. Mao, and S. Xu. 2009. NIR-responsive silica-coated $NaYbF_4$:Er/Tm/Ho upconversion fluorescent nanoparticles with tunable emission colors and their applications in immunolabeling and fluorescent imaging of cancer cells. *J. Phys. Chem. C* 113 (44):19021–19027.

Wang, X., J. Zhuang, Q. Peng, and Y. D. Li. 2005. A general strategy for nanocrystal synthesis. *Nature* 437 (7055):121–124.

Wang, Z.-L., J. H. Hao, and H. L. W. Chan. 2010. Down- and up-conversion photoluminescence, cathodoluminescence and paramagnetic properties of $NaGdF_4$: Yb^{3+}, Er^{3+} submicron disks assembled from primary nanocrystals. *J. Mater. Chem.* 20 (16):3178–3185.

Wong, H.-T., F. Vetrone, R. Naccache, H. L. W. Chan, J. Hao, and J. A. Capobianco. 2011. Water dispersible ultra-small multifunctional $KGdF_4$:Tm^{3+}, Yb^{3+} nanoparticles with near-infrared to near-infrared upconversion. *J. Mater. Chem.* 21 (41):16589–16596.

Yang, D., P. Ma, Z. Hou, Z. Cheng, C. Li, and J. Lin. 2014. Current advances in lanthanide ion (Ln^{3+})-based upconversion nanomaterials for drug delivery. *Chem. Soc. Rev.* 44:1416–1448.

Yang, P., S. Gai, and J. Lin. 2012. Functionalized mesoporous silica materials for controlled drug delivery. *Chem. Soc. Rev.* 41 (9):3679–3698.

Yang, Y., Q. Shao, R. Deng et al. 2012. *In vitro* and *in vivo* uncaging and bioluminescence imaging by using photocaged upconversion nanoparticles. *Angew. Chem. Int. Ed.* 51 (13):3125–3129.

Ye, X., J. E. Collins, Y. Kang, J. Chen, D. T. N. Chen, A. G. Yodh, and C. B. Murray. 2010. Morphologically controlled synthesis of colloidal upconversion nanophosphors and their shape-directed self-assembly. *Proc. Natl. Acad. Sci. USA* 107 (52):22430–22435.

Yi, G.-S. and G.-M. Chow. 2005. Colloidal LaF_3:Yb, Er, LaF_3:Yb, Ho and LaF_3:Yb, Tm nanocrystals with multicolor upconversion fluorescence. *J. Mater. Chem.* 15 (41):4460–4464.

Yi, G. S. and G. M. Chow. 2006. Synthesis of hexagonal-phase $NaYF_4$:Yb, Er and NaYF4:Yb, Tm nanocrystals with efficient up-conversion fluorescence. *Adv. Funct. Mater.* 16 (18):2324–2329.

Yi, G. S., H. C. Lu, S. Y. Zhao, G. Yue, W. J. Yang, D. P. Chen, and L. H. Guo. 2004. Synthesis, characterization, and biological application of size-controlled nanocrystalline $NaYF_4$: Yb, Er infrared-to-visible up-conversion phosphors. *Nano Lett.* 4 (11):2191–2196.

Yu, M., J. Lin, Z. Wang, J. Fu, S. Wang, H. J. Zhang, and Y. C. Han. 2002. Fabrication, patterning, and optical properties of nanocrystalline YVO_4:A (A = Eu^{3+}, Dy^{3+}, Sm^{3+}, Er^{3+}) phosphor films via sol–gel soft lithography. *Chem. Mater.* 14 (5):2224–2231.

Yu, X., M. Li, M. Xie, L. Chen, Y. Li, and Q. Wang. 2010. Dopant-controlled synthesis of water-soluble hexagonal $NaYF_4$ nanorods with efficient upconversion fluorescence for multicolor bioimaging. *Nano Res.* 3 (1):51–60.

Zanzoni, S., M. Pedroni, M. D'Onofrio, A. Speghini, and M. Assfalg. 2016. Paramagnetic nanoparticles leave their mark on nuclear spins of transiently adsorbed proteins. *J. Am. Chem. Soc.* 138 (1):72–75.

Zeng, J. H., J. Su, Z. H. Li, R. X. Yan, and Y. D. Li. 2005. Synthesis and upconversion luminescence of hexagonal-phase $NaYF_4$:Yb, Er^{3+} phosphors of controlled size and morphology. *Adv. Mater.* 17 (17):2119–2123.

Zeng, S., J. Xiao, Q. Yang, and J. Hao. 2012. Bi-functional $NaLuF_4$:Gd^{3+}/Yb^{3+}/Tm^{3+} nanocrystals: Structure controlled synthesis, near-infrared upconversion emission and tunable magnetic properties. *J. Mater. Chem.* 22 (19):9870–9874.

Zhang, C., J. Chen, Y. C. Zhou, and D. Q. Li. 2008. Ionic liquid-based "all-in-one" synthesis and photoluminescence properties of lanthanide fluorides. *J. Phys. Chem. C* 112 (27):10083–10088.

Zhang, Y. W., X. Sun, R. Si, L. P. You, and C. H. Yan. 2005. Single-crystalline and monodisperse LaF_3 triangular nanoplates from a single-source precursor. *J. Am. Chem. Soc.* 127 (10):3260–3261.

Zhao, J., Y. Sun, X. Kong, L. Tian, Y. Wang, L. Tu, J. Zhao, and H. Zhang. 2008. Controlled synthesis, formation mechanism, and great enhancement of red upconversion luminescence of $NaYF_4$:Yb^{3+}, Er^{3+} nanocrystals/submicroplates at low doping level. *J. Phys. Chem. B* 112 (49):15666–15672.

Zheng, K. Z., W. Y. Song, C. J. Lv, Z. Y. Liu, and W. P. Qin. 2014. Controllable synthesis and size-dependent upconversion luminescence properties of Lu_2O_3:Yb^{3+}/Er^{3+} nanospheres. *CrystEngComm* 16 (20):4329–4337.

Zhou, J., Z. Liu, and F. Li. 2012. Upconversion nanophosphors for small-animal imaging. *Chem. Soc. Rev.* 41:1323–1349.

Zhou, J., Y. Sun, X. Du, L. Xiong, H. Hu, and F. Li. 2010. Dual-modality *in vivo* imaging using rare-earth nanocrystals with near-infrared to near-infrared (NIR-to-NIR) upconversion luminescence and magnetic resonance properties. *Biomaterials* 31 (12):3287–3295.

Zhu, X., B. Da Silva, X. Zou, B. Shen, Y. Sun, W. Feng, and F. Li. 2014. Intra-arterial infusion of PEGylated upconversion nanophosphors to improve the initial uptake by tumors *in vivo*. *RSC Adv.* 4 (45):23580–23584.